Kinetic Mechanism and Enantioselectivity of Halohydrin Dehalogenase from *Agrobacterium radiobacter*†

Lixia Tang, Jeffrey H. Lutje Spelberg, Marco W. Fraaije, and Dick B. Janssen*

Laboratory of Biochemistry, Groningen Biomolecular Sciences and Biotechnology Institute, University of Groningen, Nijenborgh 4, NL-9747 AG, Groningen, The Netherlands

Received December 10, 2002; Revised Manuscript Received March 10, 2003

ABSTRACT: Halohydrin dehalogenase (HheC) from *Agrobacterium radiobacter* AD1 catalyzes the reversible intramolecular nucleophilic displacement of a halogen by a hydroxyl group in *vicinal* haloalcohols, producing the corresponding epoxides. The enzyme displays high enantioselectivity toward some aromatic halohydrins. To understand the kinetic mechanism and enantioselectivity of the enzyme, steady-state and pre-steady-state kinetic analysis was performed with *p*-nitro-2-bromo-1-phenylethanol (PNSHH) as a model substrate. Steady-state kinetic analyses indicated that the k_{cat} of the enzyme with the (*R*)-enantiomer (22 s^{-1}) is 3-fold higher than with the (*S*)-enantiomer and that the K_m for the (*R*)-enantiomer (0.009 mM) is about 45-fold lower than that for the (*S*)-enantiomer, resulting in a high enantiopreference for the (*R*)-enantiomer. Product inhibition studies revealed that HheC follows an ordered Uni Bi mechanism for both enantiomers, with halide as the first product to be released. To identify the rate-limiting step in the catalytic cycle, pre-steady-state experiments were performed using stopped-flow and rapid-quench methods. The results revealed the existence of a pre-steady-state burst phase during conversion of (*R*)-PNSHH, whereas no such burst was observed with the (*S*)-enantiomer. This indicates that a product release step is rate-limiting for the (*R*)-enantiomer but not for the (*S*)-enantiomer. This was further examined by doing single-turnover experiments, which revealed that during conversion of the (*R*)-enantiomer the rate of bromide release is 21 s^{-1}. Furthermore, multiple turnover analyses showed that the binding of (*R*)-PNSHH is a rapid equilibrium step and that the rate of formation of product ternary complex is 380 s^{-1}. Taken together, these findings enabled the formulation of an ordered Uni Bi kinetic mechanism for the conversion of (*R*)-PNSHH by HheC in which all of the rate constants are obtained. The high enantiopreference for the (*R*)-enantiomer can be explained by weak substrate binding of the (*S*)-enantiomer and a lower rate of reaction at the active site.

Halogenated organic compounds are often detected in the environment, either at low concentration because of natural production or at higher levels because of environmental pollution (*1*, *2*). Many synthetic halogenated compounds are more persistent in the environment than their nonhalogenated analogues, indicating that halogenation causes recalcitrance. Furthermore, the presence of a halogen function often causes toxicity when halogenated compounds are metabolized in higher eukaryotes because of the formation of reactive products. Thus, the study of dehalogenating enzymes is important from an environmental and toxicological point of view. Among the dehalogenating enzymes, hydrolytic dehalogenases have been studied in most detail, and their catalytic mechanism and structure have been solved by X-ray structure analysis and site-directed mutagenesis (*3*−*10*). For other dehalogenases, structural and mechanistic data are lacking.

Halohydrin dehalogenases, also referred to as haloalcohol dehalogenases or halohydrin hydrogen-halide lyases, catalyze the intramolecular nucleophilic displacement of a halogen by a hydroxyl group in *vicinal* haloalcohols, producing the corresponding epoxides. Several enzymes of this class have been expressed and purified. They play a key role in the degradation of xenobiotic environmental pollutants such as 1,2-dibromoethane and epichlorohydrin. Furthermore, because of their enantioselectivity, halohydrin dehalogenases have interesting biocatalytic potential (*11*−*14*).

Three novel bacterial genes encoding halohydrin dehalogenases were recently cloned and expressed in *Escherichia coli* by van Hylckama Vlieg et al. (*15*). The results indicate that the sequence and 3-D structure are similar to proteins of the short-chain dehydrogenase/reductase (SDR)[1] protein family. Moreover, the typical catalytic triad (Ser/Tyr/Lys) of SDR enzymes is highly conserved except for the Lys residue, which is replaced by Arg in halohydrin dehalogenases. Therefore, the catalytic mechanism of dehalogenation is predicted to share similarities to that of other enzymes in the SDR family. It has been proven by site-directed mutagenesis studies that the conserved Ser, Tyr, and Arg in

† This work was supported by Grant QLK3-2000-00426 from the EU.

* To whom correspondence should be addressed. Tel: (+31) 50-3634209. Fax: (+31) 50-3634165. E-mail: D.B.Janssen@chem.rug.nl.

[1] Abbreviations: HheC, halohydrin dehalogenase; PNSHH, *p*-nitro-2-bromo-1-phenylethanol; SDR, short-chain dehydrogenase/reductase; PNSO, *p*-nitrostyrene oxide; V_{maxc}, maximum rate for the ring-closure reaction of PNSHH; V_{maxo}, maximum rate for the ring-opening reaction of PNSO; K_{mPNSHH} and K_{iPNSHH}, Michaelis−Menten and inhibition constant for PNSHH; K_{mPNSO} and K_{iPNSO}, Michaelis−Menten and inhibition constant for PNSO; K_{mHBr} and K_{iHBr}, Michaelis−Menten and inhibition constant for HBr.

10.1021/bi0273361 CCC: $25.00
Published on Web 04/15/2003

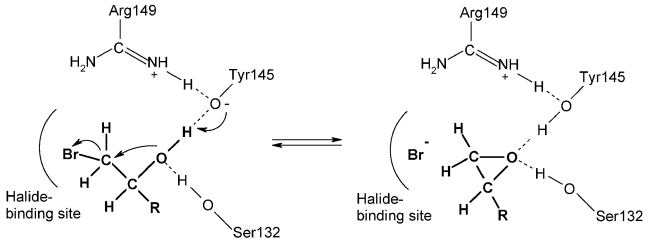

FIGURE 1: Proposed reaction mechanism of halohydrin dehalogenase from *A. radiobacter* AD1 (HheC).

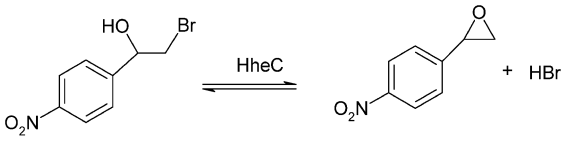

FIGURE 2: Reversible dehalogenation of PNSHH by HheC.

HheC are crucial for catalysis. A base-catalyzed mechanism is then expected with the Tyr and Arg pair involved in proton abstraction (Figure 1). Insight in the kinetic mechanism can provide further information about the sequence of reaction steps occurring at the enzyme active site and explain the observed enantioselectivity. It is also useful for rational protein engineering aimed at modifying the enzyme for biotechnologically relevant conversions.

In this study, we investigated the kinetics of halohydrin dehalogenase from *A. radiobacter* AD1 (HheC) using *p*-nitro-2-bromo-phenylethanol (PNSHH) as a model substrate (Figure 2). This is a chiral compound of which the conversion to *p*-nitrostyrene oxide can be followed using a spectrophotometer. The results suggest that the enzyme follows an ordered Uni Bi mechanism and that with (*R*)-PNSHH the release of bromide is the slowest in the catalytic cycle.

MATERIALS AND METHODS

Materials. Both enantiomers of *p*-nitro-2-bromo-1-phenylethanol (PNSHH) and *p*-nitrostyrene oxide (PNSO) were synthesized as described by Westkaemper and Hanzlik (*16*). The enantiomers of PNSHH and PNSO were separated by preparative HPLC using an analytical Chiralpak AS column with hexane/2-propanol (95:5) as eluent, which yielded product of at least 98% enantiopurity. The retention times of individual enantiomers is as follows: (*R*)-PNSHH, 25.5 min; (*S*)-PNSHH, 28.9 min; (*R*)-PNSO, 13.7 min; and (*S*)-PNSO, 18.7 min. All other chemicals were of p.a. quality.

Enzyme Purification and Assay. Halohydrin dehalogenase was expressed in *E. coli* BL21(DE3) (*17*) as described before (*18*). All buffers contained 10% glycerol and 1 mM β-mercaptoethanol to improve the stability of the enzyme (*19*). The enzyme could be stored at −70 °C for at least three months without significant loss of activity.

The activity of HheC was routinely determined by monitoring halide liberation at 30 °C using 5 mM 2-bromoethanol dissolved in 50 mM Tris/SO_4 buffer (pH 8.0) (*20*). The same assay conditions with different substrates were used for determining the substrate specificity of HheC. The concentration of protein was determined by measuring the absorbance at 280 nm. The extinction coefficient of HheC was calculated by using the program Protean in DNASTAR (ϵ_{280} = 35 920 cm^{-1} M^{-1}).

Scheme 1

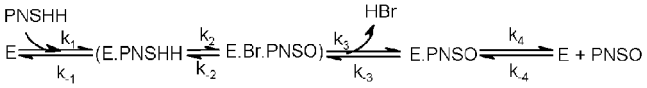

Steady-State Kinetics. The following overall velocity eq 1 that we used for the model reaction (Figure 2) describes the rate for an ordered Uni Bi mechanism (Scheme 1) (*21*):

$$V = \frac{V_{maxc}\left([PNSHH] - \frac{[HBr][PNSO]}{K_{eq}}\right)}{K_{mPNSHH} + [PNSHH] + \frac{V_{maxc}K_{mPNSO}[HBr]}{V_{maxo}K_{eq}} + \frac{V_{maxc}K_{mHBr}[PNSO]}{V_{maxo}K_{eq}} + \frac{[PNSHH][HBr]}{K_{iPNSO}} + \frac{V_{maxc}[PNSO][HBr]}{V_{maxo}K_{eq}}} \quad (1)$$

When the concentration of PNSO is 0, eq 1 can be simplified and transformed to the double-reciprocal form of Lineweaver−Burk to eq 2 with substitution of K_{eq} (Haldane equation: $K_{eq} = V_{maxc}K_{iHBr}K_{mPNSO}/(V_{maxo}K_{iPNSHH})$).

$$\frac{1}{V} = \frac{K_{mPNSHH}}{V_{maxc}}\left(1 + \frac{K_{mPNSO}[HBr]}{K_{iPNSO}K_{mHBr}}\right)\frac{1}{[PNSHH]} + \frac{1}{V_{maxc}}\left(1 + \frac{[HBr]}{K_{iHBr}}\right) \quad (2)$$

When the concentration of HBr is 0, eq 1 can be simplified to an equation for a linear-competitive inhibition:

$$\frac{1}{V} = \frac{1}{V_{maxc}} + \frac{K_{mPNSHH}}{V_{maxc}}\left(1 + \frac{[PNSO]}{K_{iPNSO}}\right)\frac{1}{[PNSHH]} \quad (3)$$

Eqs 2 and 3 were used for analyzing product inhibition. They show that in the absence of the other product PNSO acts as a competitive inhibitor and HBr acts as a S-linear I-linear mixed type inhibitor of the ring-closure reaction. When the concentration of both products is zero, eq 1 can be simplified to a Michaelis−Menten equation:

$$V = \frac{V_{maxc}[PNSHH]}{K_{mPNSHH} + [PNSHH]} \quad (4)$$

With the chromogenic substrate *p*-nitro-2-bromo-phenylethanol, the initial velocities were measured on a Perkin-Elmer Lambda Bio 10 UV−vis spectrometer by monitoring the absorbance change at 310 nm (ϵ_{PNSHH} = 3100 cm^{-1} M^{-1}; ϵ_{PNSO} = 4289 cm^{-1} M^{-1}) in 50 mM Tris/SO_4 buffer (pH 7.5) at 30 °C (*22*). As the K_m of (*R*)-PNSHH is very low and conversion proceeds rapidly, a stopped-flow apparatus (Applied Photophysics model SX17MV) was used for initial rate measurements of (*R*)-PNSHH conversion. Initial rates were determined from the initial linear part of the reaction progress curves. Kinetic data were fitted to the Michaelis−Menten eq 4.

The product inhibition pattern was obtained using initial rate methods by varying the concentration of PNSHH at several fixed concentrations of bromide. The results were plotted in double-reciprocal form, on the basis of which a product inhibition pattern was proposed.

Progress Curve Analysis. Progress curves of ring-closure reactions were measured using the stopped-flow apparatus under the same experimental conditions as in the initial rate experiments. All reactions were monitored spectrophotometrically at 310 nm until equilibrium was reached. No chemical conversion of substrate or enzyme inactivation was detected under the experimental conditions.

For fitting the experimental traces to eq 4, data sets from independent experiments were fitted simultaneously with fixing all known values of substrate and enzyme concentrations, the extinction coefficients of substrate and product, and the k_{cat} value obtained from the initial rate method. The quality of the fit and the information content of the data were checked by inspecting the standard deviation of each parameter value and the correlation between the fitting parameters using the statistics procedure implemented in the program MicroMath Scientist.

Bromide Titration Measurements. Steady-state bromide binding measurements were performed on a Fluorolog-3 spectrofluorometer at 30 °C. The excitation wavelength was 290 nm, and emission spectra were recorded in the range of 300−450 nm. Immediately prior to the experiment, the enzyme was diluted to 0.03 mg/mL. Halide ions and nucleophiles were added from freshly prepared stock solutions in 50 mM Tris-sulfate buffer (pH 8.0) containing 1 mM β-mercaptoethanol. The change in fluorescence was corrected for dilution, which did not exceed 10%. Substrate binding was analyzed from the relative change of the fluorescence intensity at λ_{Emax} (ΔF) at varying substrate concentrations. Apparent steady-state dissociation constants were obtained by nonlinear regression fitting of eq 5 using Sigmaplot 2000.

$$\Delta F = f_a[S]/([S] + K_d) \quad (5)$$

In this equation, [S] is the concentration of halide or epichlorohydrin, K_d is the apparent dissociation constant, and f_a is the relative change of the fluorescence intensity at [S] $\gg K_d$.

Stopped-Flow Experiments. All stopped-flow fluorescence experiments were done at 30 °C on an Applied Photophysics model SX17MV stopped-flow apparatus. The enzyme was excited at 290 nm, and the fluorescence emitted above 320 nm was monitored through a 320 nm cutoff filter. All experiments were performed by mixing enzyme with an equal volume of substrate solution in 50 mM Tris-sulfate buffer (pH 7.5) at 30 °C. The mentioned concentrations are the final concentration after mixing. Each trace shown is the average of 4−6 repeated experiments. Immediately prior to the experiment, the enzyme was diluted to the required concentration with 50 mM Tris-sulfate buffer (pH 7.5) containing 1 mM β-mercaptoethanol to protect the enzyme against inactivation.

The stopped-flow absorbance experiments were performed on the same equipment. For burst kinetics experiments, a 0.2 cm pathway cell was used, and the reactions were performed at 30 °C. For single turnover experiments, the reactions were monitored by following the absorbance at 310 nm under the same conditions as used for stopped-flow fluorescence experiments.

Rapid-Quench Experiments. To measure the kinetics of formation of (*R*)-PNSO from PNSHH during pre-steady-state

Scheme 2

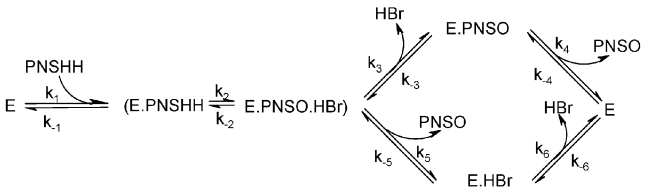

Scheme 3

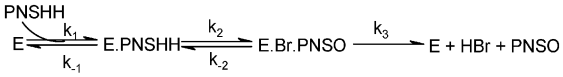

Scheme 4

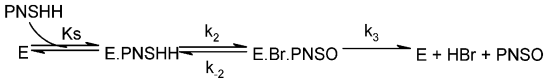

experiments, we used the RQF-63 rapid-quench apparatus from Kintek Instruments. Enzyme and (*R*)-PNSHH were mixed in the apparatus to final concentrations of 0.75 and 1.5 mM, respectively, at 30 °C. The reaction mixtures were quenched with 0.4 M H_2SO_4 (final concentration). To prevent chemical conversion of PNSO under these acidic conditions, the quenched reaction mixtures were directly injected into a tube containing 0.7 mL of 1 M phosphate buffer (pH 7.6) and 1.5 mL of diethyl ether with mesitylene as an internal standard. Quantitative analysis of PNSO in the ether phase was performed by HPLC using an analytical Chiralcel OD column with heptane/2-propanol (92:8) as eluent (1.3 mL/min). The retention times of (*R*)-PNSO and (*R*)-PNSHH were 8.3 and 16.8 min, respectively.

Data Analysis. The data from transient kinetic experiments were simulated and fitted with the program MicroMath Scientist. For burst kinetic studies, which were done at [S] $\gg K_{mPNSHH}$, the rapid-quench data were fitted with eq 6 (*23*), where λ is the observed rate constant and A_0 is the amplitude, resulting in unique solutions for λ, A_0, and k_{catc}. For the absorbance data of burst kinetic experiments, the values of λ and A_0 are very sensitive to the first few data points, which could not be measured very accurately since the burst phase was completed within the first 5 ms. Therefore, it is difficult to obtain precise values for both parameters from this measurement. Eqs 7 and 8, which give the amplitude and rate constant of the burst as a function of the rate constants in Scheme 4, were used as a check during the calculation of these rate constants from single-turnover and multiple-turnover experiments.

$$([E\bullet Br\bullet PNSO] + [PNSO])/E_{tot} = A_0(1 - e^{\lambda t}) + k_{catc}t \quad (6)$$

$$A_0 = \frac{k_2(k_2 + k_{-2})}{(k_2 + k_{-2} + k_3)(k_2 + k_{-2} + k_3)} \quad (7)$$

$$\lambda = k_2 + k_{-2} + k_3 \quad (8)$$

The fluorescence traces of the multiple-turnover experiments were fitted with a single exponential equation. The resulting observed rate constants were directly fitted with eq 9, derived from Scheme 4, to obtain a solution for the kinetic constants. The fit was constrained by the value of k_3 obtained from steady-state measurements, which was allowed

Table 1: Kinetic Parameters of Wild-Type HheC with (*R*)-PNSHH and (*S*)-PNSHH[a]

	K_{mPNSHH}[b] (μM)	k_{catc}[b] (s^{-1})	k_{catc}/K_{mPNSHH}[b] ($s^{-1}\,\mu M^{-1}$)	k_{cato}/K_{mPNS}[c] ($s^{-1}\,\mu M^{-1}$)	K_{iPNSHH}[d] (mM)	K_{iPNSO}[d] (mM)	K_{iHBr}[d] (mM)
(*R*)-PNSHH	9 ± 3	22 ± 1	2.5	0.018	0.01	$\gg 1.3$	1.0
(*S*)-PNSHH	430 ± 50	7 ± 1	0.016	0.0001	1.0	$\gg 1.3$	1.2

[a] Constants are defined in eq 1. [b] Determined by initial rate methods. [c] Calculated from the Haldane equation ($K_{eq} = k_{catc}K_{iHBr}K_{mPNSO}/(k_{cato}K_{iPNSHH})$). [d] Determined by product inhibition experiments.

Scheme 5

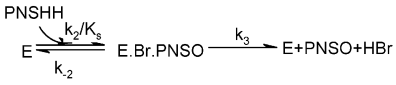

to vary within the margin of experimental error to optimize the fit.

$$k_{obs} = k_{-2} + k_3 + \frac{k_2[\text{PNSHH}]}{[\text{PNSHH}] + K_s} \quad (9)$$

The single-turnover fluorescence data and absorbance data were simultaneously fitted (Scheme 5). For this, the experimental fluorescence trace was described as the sum of the contribution of each enzyme species to the total fluorescence and absorbance trace as the sum of contributions of substrate and product. The relative fluorescence intensity of the ternary complex (E•Br•(*R*)-PNSO) was derived from the change of the fluorescence of HheC in the presence of a concentration of bromide far above its K_d value. The extinction coefficient of the E•Br•(*R*)-PNSO complex was estimated according to the burst amplitude value obtained from the absorbance burst kinetic experiments. Numerical fitting of the appropriate differential equations to the experimental data resulted in unique solutions for the kinetic constants of Scheme 5.

Equations for k_{catc} and K_{mPNSHH} according to Scheme 4 were derived using the King−Altman method described by Huang (*24*).

$$k_{catc} = \frac{k_2k_3}{k_2 + k_{-2} + k_3} \quad (10)$$

$$K_{mPNSHH} = \frac{K_s(k_{-2} + k_3)}{k_2 + k_{-2} + k_3} \quad (11)$$

RESULTS

Steady-State Kinetic Mechanism of HheC. The conversion of the chromogenic substrate *p*-nitro-2-bromo-1-phenylethanol (PNSHH) catalyzed by HheC can be monitored by following the absorbance at 310 nm (Figure 2). It has been found that HheC converts (*R*)-PNSHH preferably, yielding (*R*)-PNSO, followed by a much slower conversion of the (*S*)-enantiomer (*22*). Both of the PNSHH enantiomers were converted according to Michaelis−Menten kinetics. Initial rate measurements showed that (*R*)-PNSHH is one of the best substrates of HheC in the ring-closure reaction, with a k_{catc}/K_{mPNSHH} of 2.5×10^6 s^{-1} M^{-1} (Table 1).

The kinetic mechanism for the overall reaction can be described as a Uni Bi/Bi Uni system (Scheme 2). If the catalytic cycle follows either the upper or lower route in Scheme 2, the Uni Bi mechanism is ordered with either bromide or epoxide as the first product that is released. If both routes are followed, a random Uni Bi mechanism is obtained. As steady-state measurements provide no information about isomerization steps between intermediates that are interconverted only by a first-order reaction process (E•PNSHH ↔ E•PNSO•Br), these intermediates can be combined for obtaining steady-state kinetic equations (*21*). Since at the concentrations used the equilibrium of the conversion of PNSHH is strongly directed toward the epoxide (K_{eq} = 0.48 M) (*22*), we used the forward (ring-closure) reaction to obtain information about the kinetic mechanism.

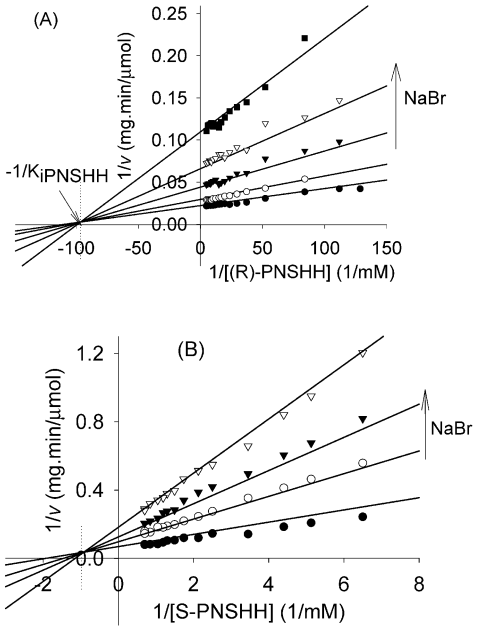

FIGURE 3: Inhibition of HheC by bromide. Panel A: double-reciprocal plots of bromide inhibition on the ring-closure reaction of (*R*)-PNSHH. (*R*)-PNSHH was varied from 0.007 to 0.1 mM at fixed concentrations of bromide: ●, 0 mM; ○, 0.25 mM; ▼, 0.75 mM; ▽, 1.5 mM; and ■, 3 mM. Panel B: double-reciprocal plots of bromide inhibition on the ring-closure reaction of (*S*)-PNSHH. (*S*)-PNSHH was varied from 0.1 to 1.6 mM at fixed concentrations of bromide: ●, 0 mM; ○, 0.5 mM; ▼, 1 mM; and ▽, 2 mM. The points are the experimentally determined values; the lines indicate the best fit to these data using eq 2.

To distinguish between an ordered Uni Bi mechanism and a random Uni Bi mechanism, the pattern of product inhibition was tested by using initial rate measurements. The addition of NaBr decreased the enzyme activity for (*R*)-PNSHH. Effects on both K_{mPNSHH} and V_{maxc} could be clearly observed at 0.5 mM NaBr. The double-reciprocal plots of these data fitted well to eq 2, corresponding to S-linear I-linear mixed-type inhibition with a single cross point that is close to the horizontal axis (Figure 3A), resulting in unique solutions for inhibition constants of (*R*)-PNSHH and bromide (Table 1). These results indicate that bromide acts as an S-linear I-linear mixed-type inhibitor in the conversion of (*R*)-PNSHH catalyzed by HheC. Consequently, bromide release does not seem to be the last step in the catalytic cycle. Applying the

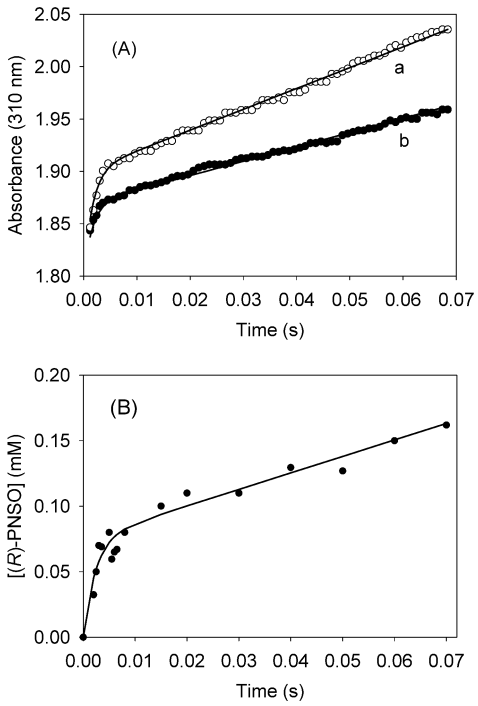

FIGURE 4: Burst kinetics of the ring-closure reaction of (*R*)-PNSHH. Panel A: the conversion of 0.75 mM (*R*)-PNSHH was monitored followed at 310 nm after mixing with 0.11 mM (a) and 0.07 mM (b) HheC in 50 mM Tris-sulfate buffer containing 1 mM β-mercaptoethanol (pH 7.5). Panel B: the conversion of 3 mM (*R*)-PNSHH by 0.07 mM HheC in 50 mM Tris-sulfate buffer containing 1 mM β-mercaptoethanol (pH 7.5) determined by rapid-quench analysis after different incubation times. The solid lines were obtained by fitting the experimental data with eq 6.

rules for product inhibition for different Uni Bi mechanisms (*25*), the inhibition pattern of bromide already excludes a random Uni Bi mechanism and suggests an ordered Uni Bi mechanism in which bromide is first released followed by PNSO release (Scheme 1). If PNSO is the last product released, it should act as a competitive inhibitor. However, PNSO did not inhibit the conversion of 0.025 mM (*R*)-PNSHH at a concentration of 0.55 mM, and very little inhibition was observed when 1.3 mM (maximum solubility) of (*R*)-PNSO was used (data not shown), suggesting that inhibition by (*R*)-PNSO is weak. Consequently, we cannot determine the inhibition pattern of (*R*)-PNSO. Moreover, its analogue *trans*-β-methylstyrene oxide also did not show significant inhibition at a concentration of 3 mM.

As not all kinetic parameters for Scheme 1 could be obtained by the initial rate method, progress curve analysis was explored. The ring-closure reactions of (*R*)-PNSHH were performed at different starting concentrations of (*R*)-PNSHH (20−80 μM). It was found that all traces could be fitted well to the simple Michaelis−Menten eq 4 with k_{catc} and K_{mPNSHH} values of 22 s^{-1} and 0.009 mM, which were already obtained from the initial rate measurements (Table 1). This suggests that because of low values of k_{-3} and k_{-4} (Scheme 1), inhibition by both PNSO and bromide of the conversion of (*R*)-PNSHH is not significant as long as the concentration of these products is below 0.08 mM.

Pre-Steady-State Analysis of Ring-Closure of (R)-PNSHH. It was tested if there is a pre-steady-state burst of formation of (*R*)-PNSO when using high enzyme concentrations (70−110 μM) and excess substrate (Figure 4). The reactions were performed on a stopped-flow apparatus by following the absorbance at 310 nm (Figure 4A) and in a rapid-quench instrument (Figure 4B). The results of both experiments displayed a fast burst phase followed by a steady-state phase. Scheme 3, with an isomerization step included and assuming that the second product is released immediately after the first one, was used for kinetic analysis. The pre-steady-state burst of formation of PNSO indicates that the rate-limiting step during the catalytic cycle occurs after the chemical isomerization step that leads to the ternary complex (Scheme 3, step 2). By fitting the rapid-quench experimental data with eq 6, the amplitude (A_0) and rate constant (λ) of the burst phase were found to be about 1 and 420 s^{-1}, respectively, and a steady-state rate of formation of (*R*)-PNSO was also obtained (20 s^{-1}), which is in good agreement with the steady-state measurement (22 s^{-1}) (Figure 4B).

By comparing the absorbance data to the rapid-quench data, the burst phase of the absorbance trace (Figure 4A) also must be due to the formation of ternary complex (E•Br•(*R*)-PNSO). The absence of a fast jump preceding the burst suggests that PNSHH in the Michaelis complex has a similar extinction coefficient as free PNSHH. From the absorbance traces, unique solutions of A_0 and λ could not be obtained without using any further constraints because of the lack of sufficient accurate data within the first 5 ms. The absorbance data could be fitted with eq 6 by fixing λ to the value obtained from rapid-quench burst kinetic experiments (Figure 4A), which gave an A_0 value of about 0.6. This low amplitude of burst can be explained by the reduced extinction coefficient of PNSO in the ternary complex as compared to the absorbance of free PNSO. Separate measurements showed that the absorbance of PNSO is indeed sensitive to its microenvironment. The ϵ value of PNSO varied from 3550 cm^{-1} M^{-1} in 50 mM KH_2PO_4/K_2HPO_4 buffer to 4290 cm^{-1} M^{-1} in Tris-SO_4 buffer. The buffer used had only a small effect on the extinction coefficient of PNSHH. It varied from 3100 cm^{-1} M^{-1} for 50 mM Tris-SO_4 buffer to 3150 cm^{-1} M^{-1} for HEPES buffer, which is in agreement with our hypothesis that free PNSHH and bound PNSHH have a similar extinction coefficient.

Multiple-Turnover Experiments. To reveal the early events in the ring-closure reaction of (*R*)-PNSHH, we performed multiple-turnover experiments under pseudo-first-order conditions. For this, 0.5 μM HheC was mixed with (*R*)-PNSHH concentrations between 5 and 260 μM, and the fluorescence was followed (Figure 5A). All stopped-flow fluorescence traces were well-described by a single-exponential function (Figure 5B). From plots of k_{obs} versus [S], it was apparent that the concentration dependence of the rate of fluorescence increase shows saturation behavior, indicating that the increase of fluorescence is caused by the unimolecular formation of E•Br•(*R*)-PNSO ternary complex rather than the bimolecular formation of the Michaelis complex and that substrate binding is a rapid equilibrium step. Moreover, all fluorescence traces clearly show a steady-state phase, which suggests that the formation of this ternary complex is followed by a rate-limiting step (i.e., bromide release). At substrate concentrations higher than 260 μM, k_{obs} could not be accurately determined because of the large decrease in amplitude by high concentrations of substrate.

Data were fitted with eq 9 obtained from Scheme 4, resulting in unique solutions for k_2 (380 s^{-1}) and K_s (0.1

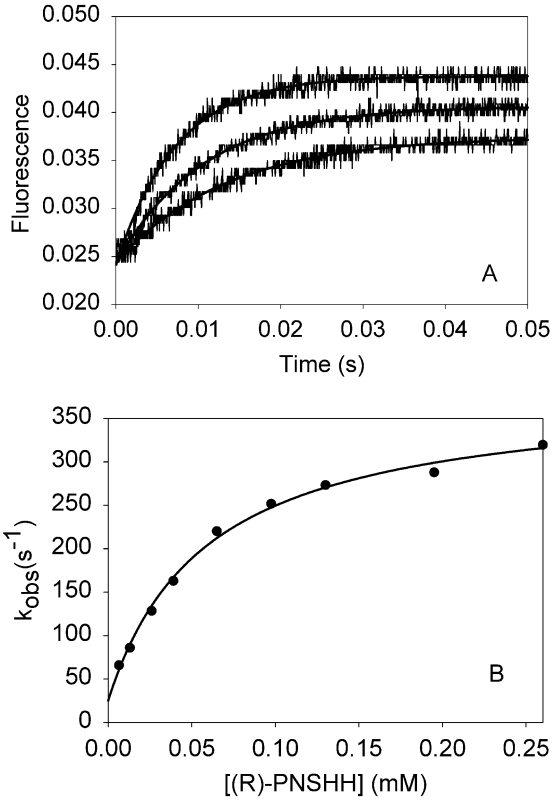

FIGURE 5: Multiple-turnover experiments with (*R*)-PNSHH. Panel A: fluorescence traces of 0.8 μM HheC with 7, 14, and 28 μM (*R*)-PNSHH at 30 °C. The solid curves show the fit of a single-exponential function to the data, resulting in k_{obs} values at different concentrations of (*R*)-PNSHH. Panel B: observed rate constants plotted as a function of (*R*)-PNSHH concentration. The solid curve is the fit of the experimental data with eq 9 using the kinetic parameters in Table 2.

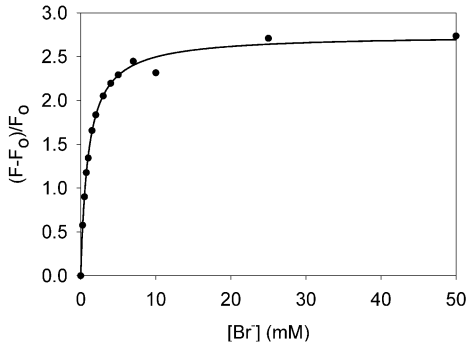

FIGURE 6: Relative fluorescence changes of HheC as a function of bromide concentration. The emission spectra were recorded at λ_{Ex} 290 nm using 0.03 mg/mL protein solutions prepared in 50 mM Tris-sulfate buffer (pH 8.0) containing 1 mM β-mercaptoethanol. The solid line is obtained by numerical fitting eq 5 to the experimental data.

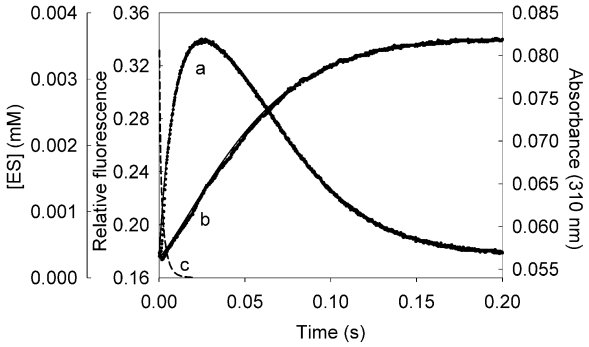

FIGURE 7: Single-turnover experiments with (*R*)-PNSHH at 30 °C. Stopped-flow fluorescence (a) and absorbance (b) traces were recorded after mixing 26.5 μM enzyme and 23.5 μM (*R*)-PNSHH. The solid lines are the best fit to the experimental data using Scheme 5 and the kinetic constants in Table 2. Curve c represents the simulated concentration of Michaelis complex using Scheme 4 and the kinetic constants in Table 2.

mM). Thus, the rate of cleavage of the carbon−halogen bond was much higher than product release (k_3), and k_3 is rate-limiting step. When k_3 was fixed to the k_{cat} value (22 s^{-1}), k_{-2} approached 3 s^{-1}.

Single-Turnover Experiments. Preliminary experiments have indicated that the fluorescence properties of HheC can be changed by binding of halide ions and other nucleophiles (N_3^- and CN^-). The fluorescence intensity of HheC was increased by adding halide. The bromide titration curve showed a saturation pattern with a K_d value of 1.2 mM (Figure 6). Thus, stopped-flow fluorescence was used to further investigate the individual steps in Scheme 3. Single-turnover experiments were performed in which 26.5 μM HheC was mixed with 23.5 μM (*R*)-PNSHH ($>K_{mPNSHH}$) at 30 °C, and the reaction was monitored by measuring tryptophan fluorescence and by following the absorbance at 310 nm (Figure 7). After mixing, the fluorescence intensity rapidly increased to a maximum within around 25 ms, followed by a slow recovery to the baseline level. As the single-turnover fluorescence trace displays two phases, a two-step mechanism is the minimal scheme needed to describe the data (Scheme 5). Multiple-turnover experiments revealed that the substrate binding step is a rapid equilibrium step; thus, the transient increase of fluorescence intensity might be caused by the formation of the E•Br•(*R*)-PNSO ternary complex and the decrease of fluorescence is likely to be caused by release of bromide ion, in agreement with the observation that the presence of bromide increased fluorescence. To further confirm that the observed fluorescence changes are attributed to those particular reaction steps, the accumulation of Michaelis complex (ES) was simulated by using Scheme 4 and the rates in Table 2 (Figure 7, curve c). It was found that only a small amount of ES accumulated and that the formation of this Michaelis complex was extremely fast, much faster than the observed increase of the fluorescence signal (Figure 7, curve a). Moreover, accumulation of a large amount of ES could only be obtained in simulations by setting the isomerization step as the slowest step in the catalytic cycle, but the burst experiments showed that it is fast. Thus, the increased fluorescence is indeed due to the formation of ternary complex rather than phase of Michaelis complex. Unlike in the fluorescence trace, there is no peak in the absorbance trace at around 25 ms where the concentration of E•Br•(*R*)-PNSO reached a maximum. Apparently, the accumulation of the E•Br•(*R*)-PNSO complex was not accompanied by a strong increase in the absorbance, indicating again that PNSO in the complex had a lower extinction coefficient constant (ϵ) than free PNSO.

Fitting of the single-turnover fluorescence and absorbance traces with Scheme 5 resulted in unique solutions for k_2/K_s (3.3 s^{-1} μM^{-1}) and for k_3 (21 s^{-1}) (Figure 7). The constraint for this fitting process was the requirement of a small value of k_{-2} (<5). The value of k_2/K_s (3.3 s^{-1} μM^{-1}) is similar to the value obtained from multiple-turnover experiments (3.8

Table 2: Kinetic Constants of Halohydrin Dehalogenase (HheC) at pH 7.5[a]

	Kinetic constants						Steady-state parameters[d]		
substrate	K_s (μM)	k_2 (s^{-1})	k_2/K_s [b] ($s^{-1}\,\mu M^{-1}$)	k_2/K_s [c] ($s^{-1}\,\mu M^{-1}$)	k_{-2} (s^{-1})	k_3 (s^{-1})	k_{catc} (s^{-1})	K_m (μM)	k_{catc}/K_m ($s^{-1}\,\mu M^{-1}$)
(*R*)-PNSHH	100 ± 9	380 ± 20	3.3 ± 0.3	3.8	3	21 ± 1	20	6.2	3.2
(*S*)-PNSHH	≥ 430	≥ 7	$-$[e]	–	–	>7	–	–	–

[a] See Scheme 4 for definition of constants. [b] Determined by single-turnover experiments. [c] Calculated using the parameter values obtained from multiple-turnover experiments. [d] Calculated from the rate constants given. [e] –: value cannot be obtained.

Table 3: Substrate Range of Halohydrin Dehalogenase

	Brominated			Chlorinated		
	K_m (μM)	k_{cat} (s^{-1})	k_{cat}/K_m ($s^{-1}\,\mu M^{-1}$)	K_m (μM)	k_{cat} (s^{-1})	k_{cat}/K_m ($s^{-1}\,\mu M^{-1}$)
X-CH_2-CH_2-OH	<200	12.4	>0.062	840	0.5	6.0×10^{-4}
X-CH_2-CH(OH)-CH_2-X	*[a]	>20	*	10	9.7	0.97
(*R*,*S*)-X-CH_2-CH(X)-CH_2-OH	<200	15.5	>0.078	820	1.0	1.2×10^{-3}
(*R*,*S*)-X-CH_2-CH(OH)-CH_2-OH	430	20.1	0.047	2200	3.7	1.7×10^{-3}
(*R*)-X-CH_2-CH(C_6H_5)-OH	–[b]	–	–	370	12.1	0.033
(*S*)-X-CH_2-CH(C_6H_5)-OH	–	–	–	4200	2.2	5.2×10^{-4}
(*R*)-X-CH_2-CH($C_6H_4NO_2$)-OH	9	22	2.5	–	–	–
(*S*)-X-CH_2-CH($C_6H_4NO_2$)-OH	430	7	0.016	–	–	–

[a] *: Compound is chemically unstable. [b] –: Compounds are not commercially available.

$s^{-1}\ \mu M^{-1}$), indicating that the conditions of those two experiments are comparable. The value of k_3 is quite close to the k_{catc} value (22 s^{-1}) of the ring-closure reaction of (*R*)-PNSHH, which means that the first product release step is rate-limiting since the single-turnover fluorescence trace is dominated by the formation and release of halide, and the absorbance trace displays the formation and release of PNSO. Taken together with the steady-state kinetics results, bromide release is proposed to be the slowest step. When the steady-state kinetic parameters (k_{catc} and K_m) were calculated by using eqs 10 and 11 derived from Scheme 4, there was good correspondence between the results obtained from transient kinetic studies and the steady-state experiments, which indicates that Scheme 4 and the corresponding rate and binding constants give a good description of the kinetic mechanism for the conversion of (*R*)-PNSHH by HheC.

Substrate Specificity and Enantioselectivity of Halohydrin Dehalogenase. The steady-state kinetic parameters for (*S*)-PNSHH were obtained by initial rate measurements (Table 1). HheC has a 45-fold higher K_m and a 3-fold lower k_{cat} for the (*S*)-enantiomer than for the (*R*)-enantiomer. The *E* value is 150 ($(k_{catc,R}/K_{mPNSHH,R})/(k_{catc,S}/K_{mPNSHH,S})$), showing that HheC prefers the (*R*)-enantiomer with very high enantioselectivity.

In product inhibition studies, bromide also acted as an I-linear S-linear mixed-type inhibitor of the conversion of (*S*)-PNHH (Figure 3B) with an inhibition constant of 1.2 mM, while (*S*)-PNSO did not show clear inhibition at a concentration of 1.3 mM. This indicates that the conversion of the (*S*)-PNSHH obeys the same kinetic mechanism as that of (*R*)-PNSHH and that halide is released first, followed by the epoxide. Moreover, the pre-steady-state kinetic experiments were also performed with 0.75 mM (*S*)-PNSHH and 0.1 mM HheC. However, there was no obvious burst phase of product formation (data not shown), which suggests that product release is not the slowest step in the catalytic cycle. This is in agreement with a 3-fold lower k_{cat} with (*S*)-PNSHH than with the (*R*)-enantiomer. Single-turnover and multiple-turnover experiments could not be performed because of the high K_m value of HheC for (*S*)-PNSHH.

The steady-state kinetics of HheC with other aromatic and aliphatic compounds was studied by using several pairs of brominated and chlorinated substrates (Table 3). It was found that (*R*)-1-phenyl-2-chloroethanol gives an 11-fold lower K_m value and a 6-fold higher k_{cat} than the (*S*)-enantiomer, resulting in an *E* value of 63. This indicates that HheC also prefers the (*R*)-enantiomer of 1-phenyl-2-chloroethanol. Moreover, all tested brominated substrates displayed a significantly lower K_m and higher k_{cat} than their chlorinated analogues. The k_{cat} values for most tested brominated aliphatic halohydrins were comparable, suggesting that they might share a similar rate-limiting step, which would be in agreement with the observation that bromide release is rate-limiting as described above. In contrast, the k_{cat} values for the tested chlorinated compounds varied significantly. HheC showed a high k_{cat} value with 1,3-dichloro-2-propanol and (*R*)-1-phenyl-2-chloroethanol, while the k_{cat} value was 10–20-fold lower for the other tested chlorinated substrates. HheC was found to be a very efficient catalyst toward 1,3-dichloro-2-propanol indicating that a different rate-limiting step may exist for other chloro alcohols, probably epoxide formation at the active site or weak substrate binding.

DISCUSSION

Halohydrin dehalogenases catalyze an unusual intramolecular substitution reaction for dehalogenation. In the proposed reaction mechanism (Figure 1), Tyr145 abstracts a proton from the hydroxyl group of the substrate, and the substrate oxygen performs a nucleophilic attack on the neighboring halogen-substituted carbon atom, resulting in the formation of epoxide and halide (*15*). The enzymes display a broad substrate range and high enantioselectivity toward some halohydrins (*12*, *13*, *15*). However, no kinetic information has been reported. To study the kinetic mechanism and understand the enantioselectivity of the enzymes, the kinetics of HheC was investigated using the ring-closure reaction of

the chromogenic substrate PNSHH. Kinetic characterization of the ring-opening reaction is complicated because of the high equilibrium constant (0.48 M) (*22*), which at practical concentrations drives the reaction in the direction of ring-closure.

Steady-state kinetic studies showed that HheC is a very efficient catalyst toward the (*R*)-enantiomer of PNSHH with a k_{catc}/K_m value of 2.5×10^6 M^{-1} s^{-1}, which is only 4−40-fold lower than some extremely efficient enzymes with a k_{cat}/K_m value range of 10^7-10^8 M^{-1} s^{-1} (*26*). The enzyme displayed a 150-fold lower catalytic efficiency for the (*S*)-enantiomer than for the (*R*)-enantiomer resulting in very high enantioselectivity. To reveal the kinetic mechanism, product inhibition experiments were performed. It is known that these can provide information about the sequence of events at the active site and the order of product release when using a double-reciprocal plot analysis (*24*, *27*, *28*). For HheC, the resulting I-linear and S-linear inhibition pattern of bromide is consistent with an ordered Uni Bi mechanism, although the inhibition pattern of PNSO could not be obtained because of its low solubility. We conclude that bromide is the first released product, followed by the epoxide (Scheme 1).

With the well-understood haloalkane dehalogenase (DhlA) from *Xanthobacter autotrophicus* GJ10 (*9*, *29*), the slowest step in the catalytic cycle is also halide release. It was found that in DhlA halide release follows a complex pathway, which involves a slow enzyme isomerization step that limits the rate of halide release. Thus, halide binding and release are separated from free enzyme by a conformational change (*30*). This explains that with DhlA halide is a noncompetitive inhibitor, even though it is the last product that is released, an explanation that has been overlooked by others (*31*). However, this cannot be the case for HheC since the single-turnover experiments revealed that the second product is released immediately after the first, indicating that the first product release step is rate-limiting. This rate-limiting step must be halide release in view of the reduction of k_{cat} by the presence of halide. In other words, if halide release would follow the release of epoxide, it should be much faster than epoxide dissociation, which is excluded by the inhibition effect of halide on k_{cat}. Haloalkane dehalogenase (DhlA) and halohydrin dehalogenase (HheC) also follow a fundamentally different mechanism. The former performs a nucleophilic attack of Asp124 on the halogen-bound carbon atom of the substrate, leading to the formation of a covalent intermediate. HheC does not form a covalent enzyme−substrate intermediate. Two tryptophan residues (Trp125 and Trp175) are found at the substrate and halide binding site of DhlA. The fluorescence of those tryptophans is quenched upon halide binding. In contrast to DhlA, the intrinsic protein fluorescence of HheC is increased when halide is bound, indicating that there is energy transfer between tryptophans that are close to the active site in the unliganded enzyme and that there is no direct interaction between a tryptophan and the halogen when substrate is bound. The proposed structure of HheC suggests that two of the three tryptophan residues are situated close to the active site, which is in agreement with strong effects of substrate binding and conversion on intrinsic protein fluorescence (*15*).

To further understand the kinetic mechanism, the pre-steady-state kinetics was investigated by stopped-flow and rapid-quench methods. A pre-steady-state burst of formation of PNSO was observed for the conversion of (*R*)-PNSHH, followed by a steady-state phase at a rate close to k_{catc}. This behavior is indicative of a mechanism in which a step after formation of PNSO is rate-limiting. The burst phase is due to the rapid formation of the product ternary complex, which indicates that the rate constant k_2 for the isomerization step is much faster than the rate of the following step, which is the release of the first product. By following the intrinsic protein fluorescence, single-turnover and a multiple-turnover experiments could be performed. The suggestion that product release is rate-limiting was confirmed by analyzing the single-turnover data, which again revealed that the k_3 (21 s^{-1}) is very close to the k_{catc} value. The multiple-turnover experiments confirmed that the unimolecular isomerization rate k_2 (380 s^{-1}) is much faster than the rate of product release, which indicates that product ternary complex accumulated during the catalytic cycle. This is the reason that the K_m value (0.009 mM) for the (*R*)-enantiomer is 10-fold lower than the substrate binding constant K_s (0.1 mM). Moreover, multiple-turnover experiments showed that substrate binding follows a rapid equilibrium, consistent with the fact that the value of k_{catc}/K_{mPNSHH} (2.5×10^6 s^{-1} M^{-1}) sets the lower limit for k_1 (*26*). A good correspondence between the results of steady-state kinetic studies and the pre-steady-state studies was achieved, indicating that Scheme 4 and the obtained kinetic parameters (Table 2) give a good description of the kinetic mechanism of conversion of the (*R*)-PNSHH by HheC.

HheC showed high enantioselectivity toward the model substrate, with an *E* value of 150. Steady-state kinetic studies revealed that the conversion of both enantiomers of PNSHH by HheC obeyed the same ordered Uni Bi mechanism with bromide release preceding epoxide release. Interestingly, unlike with (*R*)-PNSHH, no burst formation of PNSO was observed when the enzyme was mixed with excess (*S*)-PNSHH. This indicates that the conversion of (*S*)-PNSHH by HheC has a different rate-limiting step, which is in agreement with a 3-fold lower k_{cat} for (*S*)-PNSHH than that for the (*R*)-enantiomer. However, no individual rate constants could be obtained for the conversion of (*S*)-PNSHH because of its high K_m value. The high K_m of (*S*)-PNSHH indicates that the K_s (k_{-1}/k_1) value for the (*S*)-enantiomer is at least 45-fold higher than that for the (*R*)-enantiomer since the K_m value sets the lower limit for the K_s when a reaction contains at least three steps (*26*). Furthermore, the conversion of bound substrate to the ternary complex must also be slower. Similar kinetic differences may explain why HheC also preferred the (*R*)-enantiomers of other aromatic halohydrins (Table 3), which is not the case for the other two halohydrin dehalogenases that we have characterized (HheA and HheB) (*15*, *22*). The understanding of the kinetic mechanism of the conversion of the enantiomers is expected to be an important step toward modifying the selectivity of the enzyme for new biocatalytic applications.

REFERENCES

1. Krijgsheld, K. R., and van de Gen, A. (1986) Assessment of the impact of the emission of certain organochlorin compounds on the aquatic environment. Part 3: epichlorohydrin, *Chemosphere 15*, 881−893.
2. van Agteren, M. H., Kenning, S., and Janssen, D. B. (1998) *Handbook on biodegradation and biological treatment of hazard-*

ous organic compounds, Kluwer Academic Publishers, Dordrecht, The Netherlands.
3. Dong, J., Carey, P. R., Wei, Y., Luo, L., Lu, X., Liu, R. Q., and Dunaway-Mariano, D. (2002) Raman evidence for Meisenheimer complex formation in the hydrolysis reactions of 4-fluorobenzoyl- and 4-nitrobenzoyl-coenzyme A catalyzed by 4-chlorobenzoyl-coenzyme A dehalogenase, *Biochemistry 41*, 7453−7463.
4. Luo, L., Taylor, K. L., Xiang, H., Wei, Y., Zhang, W., and Dunaway-Mariano, D. (2001) Role of active site binding interactions in 4-chlorobenzoyl-coenzyme A dehalogenase catalysis, *Biochemistry 40*, 15684−15692.
5. Marek, J., Vevodova, J., Smatanova, I. K., Nagata, Y., Svensson, L. A., Newman, J., Takagi, M., and Damborsky, J. (2000) Crystal structure of the haloalkane dehalogenase from *Sphingomonas paucimobilis* UT26, *Biochemistry 39*, 14082−14086.
6. Newman, J., Peat, T. S., Richard, R., Kan, L., Swanson, P. E., Affholter, J. A., Holmes, I. H., Schindler, J. F., Unkefer, C. J., and Terwilliger, T. C. (1999) Haloalkane dehalogenases: structure of a *Rhodococcus* enzyme, *Biochemistry 38*, 16105−16114.
7. Verschueren, K. H., Franken, S. M., Rozeboom, H. J., Kalk, K. H., and Dijkstra, B. W. (1993) Refined X-ray structures of haloalkane dehalogenase at pH 6.2 and pH 8.2 and implications for the reaction mechanism, *J. Mol. Biol.* 232, 856−872.
8. Verschueren, K. H., Kingma, J., Rozeboom, H. J., Kalk, K. H., Janssen, D. B., and Dijkstra, B. W. (1993) Crystallographic and fluorescence studies of the interaction of haloalkane dehalogenase with halide ions. Studies with halide compounds reveal a halide binding site in the active site, *Biochemistry 32*, 9031−9037.
9. Verschueren, K. H., Seljee, F., Rozeboom, H. J., Kalk, K. H., and Dijkstra, B. W. (1993) Crystallographic analysis of the catalytic mechanism of haloalkane dehalogenase, *Nature 363*, 693−698.
10. Hisano, T., Hata, Y., Fujii, T., Liu, J. Q., Kurihara, T., Esaki, N., and Soda, K. (1996) Crystal structure of L-2-haloacid dehalogenase from *Pseudomonas* sp. YL: an α/β hydrolase structure that is different from the α/β hydrolase fold, *J. Biol. Chem. 271*, 20322−20330.
11. Assis, H. M., Bull, A. T., and Hardman, D. J. (1998) Synthesis of chiral epihalohydrins using haloalcohol dehalogenase A from *Arthrobacter erithii* H10a, *Enzyme Microbiol. Technol. 22*, 545−551.
12. Lutje Spelberg, J. H., van Hylckama Vlieg, J. E. T., Bosma, T., Kellogg, R. M., and Janssen, D. B. (1999) A tandem enzyme reaction to produce optically active halohydrins, epoxides, and diols, *Tetrahedron: Asymmetry 10*, 2863−2870.
13. Lutje Spelberg, J. H., van Hylckama Vlieg, J. E. T., Tang, L., Janssen, D. B., and Kellogg, R. M. (2001) Highly enantioselective and regioselective biocatalytic azidolysis of aromatic epoxides, *Org. Lett. 3*, 41−43.
14. Kasai, N., Suzuki, T., and Furukawa, Y. (1998) Chiral C3 epoxides and halohydrins: their preparation and synthetic application, *J. Mol. Catal. 4*, 237−252.
15. van Hylckama Vlieg, J. E. T., Tang, L., Lutje Spelberg, J. H., Smilda, T., Poelarends, G. J., Bosma, T., van Merode, A. E. J., Fraaije, M. W., and Janssen, D. B. (2001) Halohydrin dehalogenases are structurally and mechanistically closely related to short-chain dehydrogenases/reductases, *J. Bacteriol. 183*, 5058−5066.
16. Westkaemper, R. B., and Hanzlik, R. P. (1981) Mechanistic studies of epoxide hydrolase utilizing a continuous spectrophotometric assay, *Arch. Biochem. Biophys. 208*, 195−204.
17. Studier, F. W., Rosenberg, A. H., Dunn, J. J., and Dubendorff, J. W. (1990) Use of T7 RNA polymerase to direct expression of cloned genes, *Methods Enzymol. 185*, 60−89.
18. Rink, R., Fennema, M., Smids, M., Dehmel, U., and Janssen, D. B. (1997) Primary structure and catalytic mechanism of epoxide hydrolase from *Agrobacterium radiobacter* AD1, *J. Biol. Chem. 272*, 14650−14657.
19. Tang, L., van Hylckama Vlieg, J. E. T., Lutje Spelberg, J. H., Fraaije, M. W., and Janssen, D. B. (2002) Improved stability of halohydrin dehalogenase from *Agrobacterium radiobacter* AD1 by replacement of cysteine residues, *Enzyme Microbiol. Technol. 30*, 251−258.
20. Bergmann, J. G., and Sanik, J. (1957) Determination of trace amounts of chlorine in naphtha, *Anal. Chem. 29*, 241−243.
21. Segel, I. H. (1975) *Enzyme kinetics*: *behavior and analysis of rapid equilibrium and steady-state enzyme systems*, Wiley, New York.
22. Lutje Spelberg, J. H., Tang, L., van Gelder, M., Kellogg, R. M., and Janssen, D. B. (2002) Exploration of the biocatalytic potential of a halohydrin dehalogenase using chromogenic Substrates, *Tetrahedron: Asymmetry 13*, 1083−1089.
23. Jonson, K. A. (1992) *The enzymes* (Boyer, P. D., Ed.), 4th ed., Vol. 20, pp 1−60, Academic Press, New York.
24. Huang, C. Y. (1979) Derivation of initial velocity and isotope exchange rate equations, *Methods Enzymol. 63*, 54−84.
25. Bauer, M., Griengl, H., and Steiner, W. (1999) Kinetic studies on the enzyme (*S*)-hydroxynitrile lyase from *Hevea brasiliensis* using initial rate methods and progress curve analysis, *Biotechnol. Bioeng. 62*, 20−29.
26. Fersht, A. R. (1985) *Enzyme structure and mechanism*, 2nd ed., W. H. Freeman, New York.
27. Cleland, W. W. (1963) The kinetics of enzyme-catalyzed reactions with two or more substrates or products: III. Prediction of initial velocity and inhibition patterns by inspection, *Biochim. Biophys. Acta 67*, 188−196.
28. Lewendon, A., Murray, I. A., Shaw, W. V., Gibbs, M. R., and Leslie, A. G. (1994) Replacement of catalytic histidine-195 of chloramphenicol acetyltransferase: evidence for a general base role for glutamate, *Biochemistry 33*, 1944−1950.
29. Pries, F., Kingma, J., Krooshof, G. H., Jeronimus-Stratingh, C. M., Bruins, A. P., and Janssen, D. B. (1995) Histidine 289 is essential for hydrolysis of the alkyl-enzyme intermediate of haloalkane dehalogenase, *J. Biol. Chem. 270*, 10405−10411.
30. Schanstra, J. P., Kingma, J., and Janssen, D. B. (1996) Specificity and kinetics of haloalkane dehalogenase, *J. Biol. Chem. 271*, 14747−14753.
31. Schindler, J. F., Naranjo, P. A., Honaberger, D. A., Chang, C. H., Brainard, J. R., Vanderberg, L. A., and Unkefer, C. J. (1999) Haloalkane dehalogenases: steady-state kinetics and halide inhibition, *Biochemistry 38*, 5772−5778.

BI0273361